



## A physics-based model explains the prion-like features of neurodegeneration in Alzheimer's disease, Parkinson's disease, and amyotrophic lateral sclerosis

Johannes Weickenmeier<sup>a</sup>, Mathias Jucker<sup>b</sup>, Alain Goriely<sup>c</sup>, Ellen Kuhl<sup>d,\*</sup>

<sup>a</sup> Department of Mechanical Engineering, Stevens Institute of Technology, Hoboken, NJ 07030, USA

<sup>b</sup> Department of Cellular Neurology, Hertie-Institute for Clinical Brain Research, University of Tübingen / DZNE, German Center for Neurodegenerative Diseases, D-72076 Tübingen, Germany

<sup>c</sup> Mathematical Institute, University of Oxford, Oxford, OX2 6GG, UK

<sup>d</sup> Department of Mechanical Engineering and Stanford Neurosciences Institute, Stanford University, Stanford, CA 94305, USA



### ARTICLE INFO

#### Article history:

Received 14 August 2018

Revised 3 October 2018

Accepted 15 October 2018

Available online 15 October 2018

#### Keywords:

Continuum modeling

Reaction diffusion

Neurodegeneration

Prion

Biomarker

### ABSTRACT

Prion disease is characterized by a chain reaction in which infectious misfolded proteins force native proteins into a similar pathogenic structure. Recent studies have reinforced the hypothesis that the prion paradigm—the templated growth and spreading of misfolded proteins—could help explain the progression of a variety of neurodegenerative disorders. However, our current understanding of prion-like growth and spreading is rather empirical. Here we show that a physics-based reaction-diffusion model can explain the growth and spreading of misfolded protein in Alzheimer's disease, Parkinson's disease, and amyotrophic lateral sclerosis. To characterize the progression of misfolded proteins across the brain, we combine the classical Fisher–Kolmogorov equation for population dynamics with an anisotropic diffusion model and simulate misfolding across a sagittal section and across the entire brain. In a systematic sensitivity analysis, we probe the role of the individual model parameters and show that the misfolded protein concentration is sensitive to the coefficients of growth, extracellular diffusion, and axonal transport, to the axonal fiber orientation, and to the initial seeding region. Our model correctly predicts amyloid- $\beta$  deposits and tau inclusions in Alzheimer's disease,  $\alpha$ -synuclein inclusions in Parkinson's disease, and TDP-43 inclusions in amyotrophic lateral sclerosis and displays excellent agreement with the histological patterns in diseased human brains. When integrated across the brain, our concentration profiles result in biomarker curves that display a striking similarity with the sigmoid shape and qualitative timeline of clinical biomarker models. Our results suggest that misfolded proteins in various neurodegenerative disorders grow and spread according to a universal law that follows the basic physical principles of nonlinear reaction and anisotropic diffusion. Our findings substantiate the notion of a common underlying principle for the pathogenesis of a wide variety of neurodegenerative disorders, the prion paradigm. A more quantitative understanding of the growth and spreading of misfolded amyloid- $\beta$ , tau,  $\alpha$ -synuclein, and TDP-43 would allow us to establish a prognostic time-

\* Corresponding author.

E-mail address: [ekuhl@stanford.edu](mailto:ekuhl@stanford.edu) (E. Kuhl).

frame of disease progression. This could have important clinical implications, ranging from more accurate estimates of the socioeconomic burden of neurodegeneration to a more informed design of clinical trials and pharmacological intervention.

© 2018 The Authors. Published by Elsevier Ltd.  
This is an open access article under the CC BY license.  
(<http://creativecommons.org/licenses/by/4.0/>)

## 1. Motivation

Neurodegeneration will undoubtedly become a major challenge in medicine and public health because of demographic changes worldwide. More than 45 million people are living with dementia today and this number is expected to triple by 2050 ([World Alzheimer Report, 2016](#)). A major challenge of age-related neurodegenerative diseases is that the initial symptoms of cognitive decline become noticeable only one or two decades after the first pathological abnormalities have started to affect the brain ([Villemagne et al., 2013](#)). For several decades, researchers have tried to establish early predictive indicators of neurodegeneration and identify common pathological themes of neurodegenerative disorders. Recent evidence suggests that the key to understanding common features of neurodegeneration could lie in the unusual biology of prion diseases ([Jucker and Walker, 2018](#)). Prions, proteinaceous infectious particles, are unconventional infectious agents that consist of misfolded proteins that act as corruptive seeds to initiate a chain-reaction of misfolding, growth, and spreading ([Prusiner, 1998](#)). Prion diseases have some unique kinetic features: Disease progression is inevitable after initial seeding; the duration of the incubation period depends on both the initial seeding concentration and the rate at which prions amplify; and disease progression is characterized by a long, clinically silent incubation period during which prions grow and spread, followed by a brief and invariably fatal clinical disease ([Masel et al., 1999](#)). Interestingly, these characteristics are similar to the progression of a wide variety of age-related neurodegenerative disorders including Alzheimer's disease, Parkinson's disease, and amyotrophic lateral sclerosis ([Walker and Jucker, 2015](#)). While the clinical and pathological symptoms of these disparate disorders may vary, at the molecular level, they share with prions the unique properties of nucleation, templating, growth, and spreading ([Stopschinski and Diamond, 2017](#)). Each of these phenomena presents a potential target for therapeutic intervention ([Jucker and Walker, 2013](#)); yet, our quantitative understanding of protein misfolding remains rather limited.

[Fig. 1](#) illustrates the characteristic progression patterns of specific misfolded proteins in Alzheimer's disease, Parkinson's disease, and amyotrophic lateral sclerosis ([Jucker and Walker, 2013](#)). Interestingly, the post-mortem analysis of hundreds of human brains reveals a stereotypic progression of repeatable and predictable patterns: Amyloid- $\beta$  deposits in Alzheimer's disease shown in orange in the first row first appear in the neocortex from where they spread into the allocortex and the subcortical regions ([Thal et al., 2002](#)); tau inclusions in Alzheimer's disease shown in blue in the second row occur first in the locus coeruleus and transentorhinal layer and then spread into the amygdala and interconnected neocortical brain regions ([Braak and Braak, 1991](#));  $\alpha$ -synuclein inclusions in Parkinson's disease shown in red in the third row first occur in the dorsal motor nucleus and in the anterior olfactory nucleus from where they expand in related areas evolving the brain stem and the cortex ([Braak et al., 2003](#)); TAR DNA-binding protein-43, TDP-43, inclusions in amyotrophic lateral sclerosis shown in green in the fourth row develop first in the agranular motor cortex, brainstem motor nuclei of cranial nerves, and spinal cord motoneurons, and then spread into the prefrontal neocortex, the brainstem, the postcentral neocortex and the striatum ([Brettschneider et al., 2013](#)). These stereotypical patterns suggest that axonal transport plays a major role in the spreading of misfolded protein ([Jucker and Walker, 2011](#)). While the repeatable and predictive patterning is beginning to shape our understanding of the ontogeny of neurodegenerative disorders, there is currently no physics-based model of neurodegeneration that provides a sound quantitative explanation of the underlying spreading mechanisms.

Modeling neurodegeneration is an open problem ([Goriely et al., 2015](#)). The prion paradigm could hold the key to design physics-based models that explain the stereotypic features of neurodegenerative disorders. A consistent model must explain why the disease progresses inevitably after inoculation, why the early stages of disease progress so slowly, and why a single infectious particle will spread and ultimately cause disease unless it is rapidly degraded ([Masel et al., 1999](#)). Three different models have been proposed to simulate the kinetics of prion disease ([Pöschel et al., 2003](#)): the monomeric seeding model in which a single misfolded protein induces the misfolding of a single healthy protein ([Cohen et al., 1994](#)); the co-operative autocatalysis model in which a mixed aggregate of misfolded and healthy proteins induces misfolding of single healthy proteins ([Eigen, 1996](#)); and the polymeric seeding model, in which the misfolded protein is polymeric and induces the misfolding of a monomeric single healthy protein ([Jarrett and Lansbury, 1993](#)). Rather than choosing between the monomeric and polymeric seeding models ([Aguzzi et al., 2001](#)) as illustrated in [Fig. 2](#), the objective of this study is to establish the simplest possible model that can explain the common features of various types of neurodegenerative disorders: the growth and spreading of misfolded proteins.

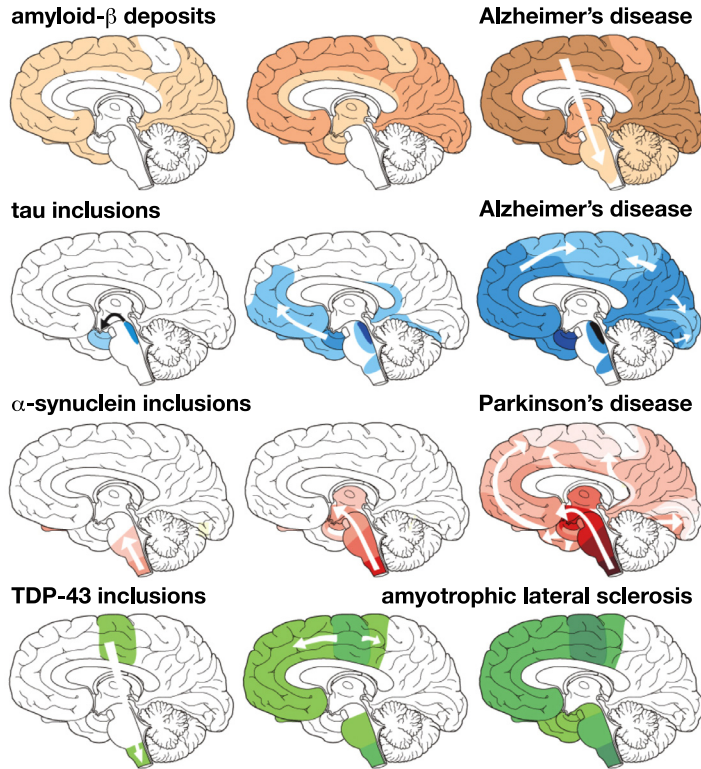


**Fig. 1.** Motivation. Commonalities among age-related neurodegenerative disorders. Characteristic progression of specific proteinaceous lesions in neurodegenerative diseases over time inferred from post-mortem analyses of brains. Amyloid- $\beta$  deposits in Alzheimer's disease; tau inclusions in Alzheimer's disease;  $\alpha$ -synuclein inclusions in Parkinson's disease; and TDP-43 inclusions in amyotrophic lateral sclerosis. Three stages of progressive neurodegeneration, from left to right, with white arrows indicating the putative spread of the lesions; adopted with permission from Jucker and Walker (2013).

## 2. Methods

### 2.1. Kinetics of prion-like spreading

To motivate our model for prion-like spreading, we consider the simplest possible kinetic representation that accounts for two configurations of the protein, the natural healthy state  $p$  and the misfolded state  $\tilde{p}$ . In this model, misfolded proteins recruit healthy proteins at a rate  $k_{11'}$ , healthy proteins bind to misfolded proteins and adopt their misfolded conformation at a rate  $k_{1'2'}$ , and the proteins fragment into misfolded infectious seeds at a rate  $k_{2'2}$ ,



It is still not entirely known whether this conformational conversion from the healthy state  $p$  to the misfolded state  $\tilde{p}$  is best represented through the *monomeric seeding model* in which the healthy protein misfolds on a single monomeric misfolded protein to first form a heterodimer, then a homodimer, and then these homodimers aggregate to amyloid, or through the *polymeric seeding model* in which misfolded proteins first organize in highly ordered polymeric infectious seeds, then recruit healthy proteins that misfold on several misfolded proteins, and then aggregate to amyloid (Scheckel and Aguzzi, 2018). Here we collectively represent both models through a single kinetic equation that simply represents the conformational conversion from the healthy to the misfolded state through the rate constant  $k_{12}$  according to Fig. 2,



We can then formulate the governing equations for the total amount of healthy protein  $p$  and misfolded protein  $\tilde{p}$ ,

$$\begin{aligned} \frac{dp}{dt} &= \text{Div}(\mathbf{D}_p \cdot \nabla p) + k_0 - k_1 p - k_{12} p\tilde{p} \\ \frac{d\tilde{p}}{dt} &= \text{Div}(\mathbf{D}_{\tilde{p}} \cdot \nabla \tilde{p}) - \tilde{k}_1 \tilde{p} + k_{12} p\tilde{p} \end{aligned} \quad (3)$$

where  $\mathbf{D}_p$  and  $\mathbf{D}_{\tilde{p}}$  characterize the spreading of  $p$  and  $\tilde{p}$ ,  $k_0$  is the production rate of the healthy protein  $p$ ,  $k_1$  and  $\tilde{k}_1$  are the clearance rates of  $p$  and  $\tilde{p}$ , and  $k_{12}$  is the conversion rate from the healthy to the misfolded conformation. This implies that

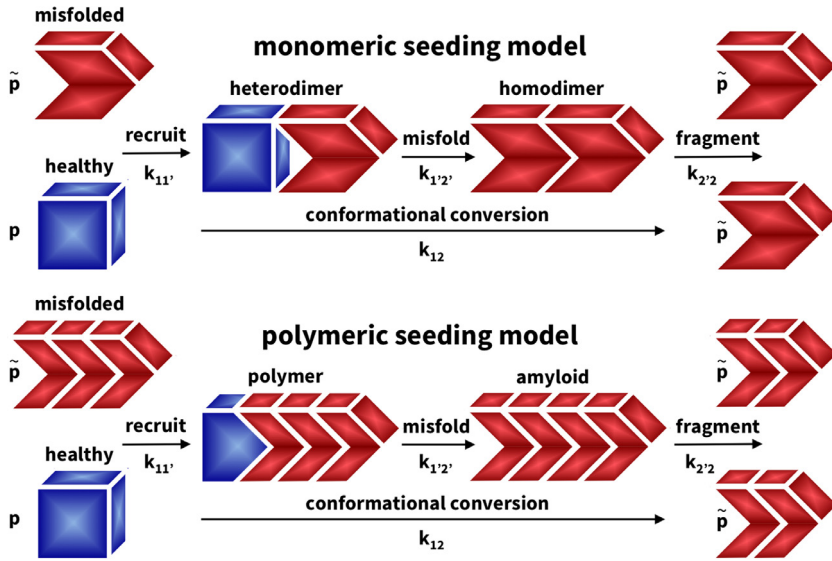


**Fig. 2.** Kinetics of prion-like spreading. In the monomeric seeding model, a healthy protein misfolds on a single misfolded protein to first form a heterodimer, then a homodimer, and then these homodimers fragment or aggregate to amyloid. In the polymeric seeding model, misfolded proteins first organize in highly ordered infectious seeds, then recruit healthy proteins that misfold on several misfolded proteins, and then fragment or aggregate to amyloid. The rate constant  $k_{12}$  collectively represents these processes as the conformational conversion from the healthy state  $p$  to the misfolded state  $\tilde{p}$ .

in the healthy state, the equilibrium concentration of healthy protein is simply  $p_0 = k_0/k_1$ . Initially, the amount of healthy protein is much larger than the amount of misfolded protein,  $p \gg \tilde{p}$ , which implies that  $dp/dt \approx 0$  and  $\text{Div}(\mathbf{D}_p \cdot \nabla p) \approx 0$ . With these assumptions, Eq. (3.1) provides an explicit estimate of the amount of healthy protein  $p$ ,

$$k_0 - k_1 p - k_{12} p \tilde{p} = 0 \quad \text{thus} \quad p = \frac{k_0}{k_1 + k_{12} \tilde{p}}. \quad (4)$$

We now approximate the healthy protein concentration  $p$  using a Taylor series evaluated at  $k_{12}/k_1 \tilde{p} = 0$ , to obtain  $p = k_0/k_1 [1 - \tilde{p} k_{12}/k_1]$ , which we substitute into Eq. (3.2),

$$\frac{d\tilde{p}}{dt} = \text{Div}(\mathbf{D}_{\tilde{p}} \cdot \nabla \tilde{p}) + \left[ k_{12} \frac{k_0}{k_1} - \tilde{k}_1 \right] \tilde{p} - \frac{k_{12}^2 k_0}{k_1^2} \tilde{p}^2. \quad (5)$$

We re-parameterize Eq. (5) in terms of the misfolded protein concentration  $c$ , which we assume to vary between zero and one,  $0 \leq c \leq 1$ , such that

$$c = \frac{\tilde{p}}{\tilde{p}^{\max}} \quad \text{with} \quad \tilde{p}^{\max} = \frac{k_1^2}{k_{12}^2 k_0} \left[ k_{12} \frac{k_0}{k_1} - \tilde{k}_1 \right]. \quad (6)$$

This results in the following partial differential equation for the misfolded protein concentration  $c$ ,

$$\frac{dc}{dt} = \text{Div}(\mathbf{D} \cdot \nabla c) + \alpha c [1 - c] \quad \text{with} \quad \alpha = k_{12} \frac{k_0}{k_1} - \tilde{k}_1, \quad (7)$$

where  $\mathbf{D} = \mathbf{D}_{\tilde{p}}$  denotes the spreading of misfolded protein that can be either purely isotropic, such that  $\text{Div}(\mathbf{D} \cdot \nabla c) = d \nabla c$ , or anisotropic along pronounced communication networks within the brain. Importantly, in this model, the growth rate  $\alpha$  of the misfolded protein concentration  $c$  increases linearly with the conversion rate from the healthy to the misfolded conformation  $k_{12}$  and with the equilibrium concentration of healthy protein  $p_0 = k_0/k_1$ , and decreases linearly with the clearance rate  $\tilde{k}_1$ .

## 2.2. Continuum model of prion-like spreading

A classical hallmark of prion-like diseases is the *growth* and *spreading* of misfolded proteins. To model the physics of prion-like diseases, we adopt Eq. (7), which is known in mathematical biology as the Fisher–Kolmogorov equation. The Fisher–Kolmogorov equation is a popular nonlinear reaction-diffusion equation that was initially proposed to model the spreading of a favored gene in population dynamics (Fisher, 1937; Kolmogorov et al., 1937). Today, the Fisher–Kolmogorov equation is widely used to describe traveling wave solutions in ecology, physiology, combustion, crystallization, plasma

physics, and phase transition. It is a natural extension of the logistic growth population model in which a population disperses via linear diffusion (Murray, 2002).

$$\frac{dc}{dt} = \text{Div}(\mathbf{D} \cdot \nabla c) + \alpha c [1 - c]. \quad (8)$$

In our case of prion-like diseases,  $c$  represents the relative concentration of misfolded protein,  $\alpha$  characterizes the growth of the concentration, and  $\mathbf{D}$  its spreading. The Fisher–Kolmogorov equation has two steady state solutions, an unstable steady state at  $c = 0$  and a stable steady state at  $c = 1$ . This implies that once misfolded protein is present anywhere in the brain,  $c > 0$ , the concentration will always be repelled from the benign state,  $c = 0$ , and attracted to the misfolded state,  $c = 1$ . We can model the seeding of misfolded protein via non-homogeneous initial conditions,  $c_0 > 0$ , in specific brain regions. Once seeded, misfolded protein can spread across the brain by two distinct mechanisms, *extracellular diffusion* and *axonal transport*. Here we associate extracellular diffusion  $d^{\text{ext}}$  with the isotropic diffusion of misfolded protein through the extracellular space and axonal transport  $d^{\text{axn}}$  with the anisotropic diffusion of misfolded protein along the local axonal direction  $\mathbf{n}$ ,

$$\mathbf{D} = d^{\text{ext}} \mathbf{I} + d^{\text{axn}} \mathbf{n} \otimes \mathbf{n}. \quad (9)$$

Prions are known to be conveyed with high specificity along established anatomical pathways and it is generally assumed that axonal transport is faster than extracellular diffusion,  $d^{\text{axn}} \geq d^{\text{ext}}$ .

### 2.3. Computational model of prion-like spreading

To solve the prion Eq. (8), we convert it into its residual format,  $R = d_t c - \text{Div}(\mathbf{D} \cdot \nabla c) - \alpha c [1 - c] \doteq 0$ , and solve it computationally using MATLAB. The basis of our solution is the weak form of the residual  $R$ , which we obtain by multiplying  $R$  with the test function  $w$ , integrating it over the domain of interest  $\mathcal{B}$ , performing the integration by parts, and including homogeneous Neumann boundary conditions,  $\nabla c \cdot \mathbf{n} = 0$ . We then discretize the weak form of the prion equation in time by partitioning the time interval of interest  $\mathcal{T}$  into  $n_{\text{step}}$  discrete time steps,  $\mathcal{T} = \bigcup_{n=1}^{n_{\text{step}}} [t_n, t]$ , where the subscript  $(\circ)_n$  is associated with the beginning of the current time step and no subscript  $(\circ) = (\circ)_{n+1}$  is associated with its end. We assume that we know the concentration of misfolded protein  $c_n$  at the beginning of the time step  $t_n$  and advance it in time using an implicit Euler backward scheme. We evaluate the prion equation at the end of the current time step  $t = t_{n+1}$  and approximate the first order time derivative of the concentration  $d_t c$  using finite differences,  $d_t c = [c_{n+1} - c_n]/\Delta t$ , where  $\Delta t := t - t_n > 0$  denotes the time step size. To discretize the prion equation in space, we partition the domain of interest  $\mathcal{B}$  into  $n_{\text{el}}$  finite elements,  $\mathcal{B} = \bigcup_{e=1}^{n_{\text{el}}} \mathcal{B}_e$  and adopt an element-wise interpolation of the test functions,  $w = \sum_{i=1}^{n_{\text{en}}} N_i w_i$ , and trial functions,  $c = \sum_{j=1}^{n_{\text{en}}} N_j c_j$ , where  $N_i$  and  $N_j$  are the finite element shape functions. Essentially, we solve the discrete weak form of the residual,

$$R_I = \sum_{e=1}^{n_{\text{el}}} \int_{\mathcal{B}_e} N_i \frac{1}{\Delta t} [c - c_n] + \nabla N_i \cdot \mathbf{D} \cdot \nabla c - N_i \alpha c [1 - c] dV \doteq 0_I, \quad (10)$$

where the operator  $A_{e=1}^{n_{\text{el}}}$  denotes the assembly of the element residuals at the  $n_{\text{en}}$  element nodes  $i$  and  $j$  to the  $n_{\text{np}}$  global nodes  $I$  and  $J$ . To solve the discrete residual, we adopt an incremental iterative Newton–Raphson solver and consistently linearize the residual (10),  $R_I^{k+1} = R_I^k + \sum_{j=1}^{n_{\text{np}}} K_{IJ} \cdot dc_j \doteq 0$ , where  $K_{IJ}$  is the global stiffness matrix,

$$K_{IJ} = \frac{dR_I}{dc_J} = \sum_{e=1}^{n_{\text{el}}} \int_{\mathcal{B}_e} N_i \frac{1}{\Delta t} N_j + \nabla N_i \cdot \mathbf{D} \cdot \nabla N_j - N_i \alpha [1 - 2c] N_j dV. \quad (11)$$

Solving the linearized residual equation,  $dc_J = -\sum_{J=1}^{n_{\text{np}}} K_{JJ}^{-1} \cdot R_I^k$ , provides the iterative update of the misfolded protein concentration,  $c_J \leftarrow c_J + dc_J$ , at all  $n_{\text{np}}$  global nodes  $J$ . Throughout this work, we use a linear finite element approximation for the misfolded protein concentration  $c$ , linear elements for the one-dimensional examples, linear triangles for the two-dimensional examples, and linear tetrahedral elements for the three-dimensional examples.

### 2.4. Illustration of prion-like spreading

[Fig. 3](#) illustrates the mechanism of prion-like spreading in neurodegeneration as predicted by the Fisher–Kolmogorov Eq. (8). For the simulation, we discretized our one-dimensional domain  $\mathcal{B} = \{x \mid -1 \leq x \leq +1\}$  with  $n_{\text{el}} = 200$  linear one-dimensional finite elements in space and our time interval  $\mathcal{T} = \{t \mid 0 \leq t \leq 20\}$  with  $n_{\text{step}} = 200$  finite difference steps of  $\Delta t = 0.1$  in time. In a preliminary convergence study, we had systematically varied the time step size between  $[\Delta t/4, \Delta t/2, \Delta t, 2\Delta t, 3\Delta t, 4\Delta t]$  with  $\Delta t = 0.1$ , for a growth of  $\alpha = 2$  and a spreading of  $d = 0.0002$ , and confirmed that the solution had converged for  $\Delta t = 0.1$ , while we observed a spurious increase in spreading for larger time step sizes. We then varied the growth as  $[1\alpha, 2\alpha, 4\alpha]$  with  $\alpha = 1$  and the spreading as  $[1d, 2d, 4d]$  with  $d = 0.0001$ , all non-dimensionalized. The initial concentration is  $c_0 = 0.0$  throughout the entire domain except for the center node at  $x = 0$ , where we seed misfolded protein at a concentration of  $c_0 = 0.1$ . Our simulations confirm that increasing the growth  $\alpha$ , from left to right, increases the local concentration of misfolded protein and *indirectly* causes a faster spreading, while increasing the spreading  $d$ , from top to bottom, *directly* causes a faster spreading of misfolded protein. The Fisher–Kolmogorov equation captures the characteristic features of prion-like diseases: (i) disease progression is inevitable after initial seeding,  $c \rightarrow 1.0$  if  $c_0 > 0.0$ ; (ii) the

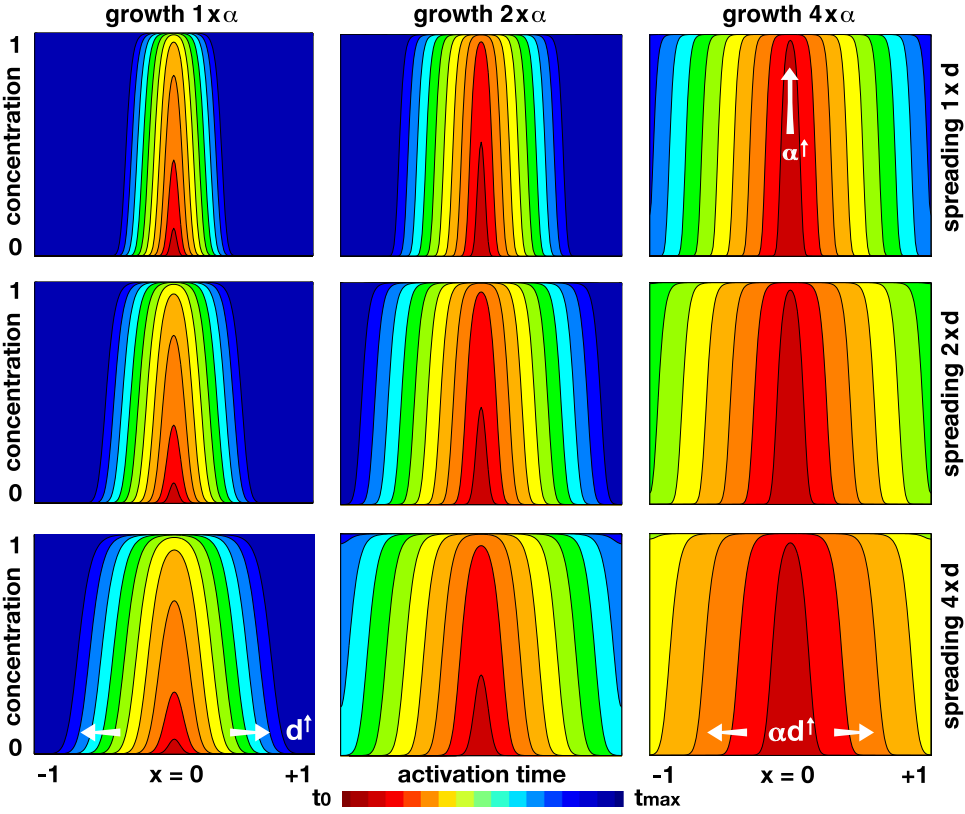


**Fig. 3.** Prion-like spreading in neurodegeneration. One-dimensional illustration of the Fisher–Kolmogorov equation and its sensitivity with respect to the growth  $\alpha$  and the spreading  $d$ . Increasing the growth  $\alpha$ , from left to right, increases the local concentration of misfolded protein and *indirectly* causes a faster spreading. Increasing the spreading  $d$ , from top to bottom, *directly* causes a faster spreading of misfolded protein.

duration of the incubation period depends on both the initial concentration of seeds,  $c_0$ , and the production rate,  $\alpha$ , of misfolded protein by the host, (iii) disease progression is characterized by an extremely long, clinically silent incubation period,  $0.0 < c < c^{\text{crit}}$ , during which the disease gradually amplifies locally, followed by a rapid local increase towards  $c = 1.0$ , and a global spreading from the initial seeding region,  $x = 0$ , across the entire domain,  $-1 \leq x \leq +1$ . Our sensitivity study in Fig. 3 confirms that the classical Fisher–Kolmogorov equation is capable of modeling these observations and explains why the disease progresses inevitably after inoculation, why the incubation period can be extremely long, and why a single infectious seed will spread and ultimately cause disease unless it is rapidly degraded (Jucker and Walker, 2013).

## 2.5. Brain models

Fig. 4 illustrates the finite element models for our simulations. To simulate prion-like spreading across the brain, we created two brain models: a fully three-dimensional whole model, and, for parametric studies, a two-dimensional sagittal model. We generated both models from T2-weighted magnetic resonance images of a healthy, 32-year old male using Simpliceware. Our two-dimensional sagittal model has 6454 nodes, 6454 concentration degrees of freedom, and 11,883 triangular elements of which 6182 are gray and 5701 are white matter. Our three-dimensional whole brain model has 79,826 nodes, 79,826 concentration degrees of freedom, and 395,409 linear tetrahedral elements of which 237,118 are gray and 158,291 are white matter.

## 2.6. Fiber models

Figs. 5 and 6 show the fiber models used in our two-dimensional sensitivity analysis and in our fully three-dimensional whole brain simulation. We model the spreading of misfolded protein through the diffusion tensor,  $\mathbf{D} = d^{\text{ext}}\mathbf{I} + d^{\text{axn}}\mathbf{n} \otimes \mathbf{n}$ , where  $d^{\text{ext}}$  is the isotropic extracellular diffusion and  $d^{\text{axn}}$  is the anisotropic axonal transport along the axonal fiber direction  $\mathbf{n}$ . In two dimensions, we probe the importance of the fiber orientation  $\mathbf{n}$  and perform a systematic sensitivity analysis using the sagittal model of Fig. 4. We compare four different cases, isotropic diffusion and anisotropic diffusion with circumferential, radial, and axon-based fiber orientations  $\mathbf{n}$ . We analytically parameterize the axonal orientation  $\mathbf{n}$  and assign 11,883 discrete fiber orientations, one for each element. Fig. 5 illustrates the fiber orientations for our circumferential, radial,

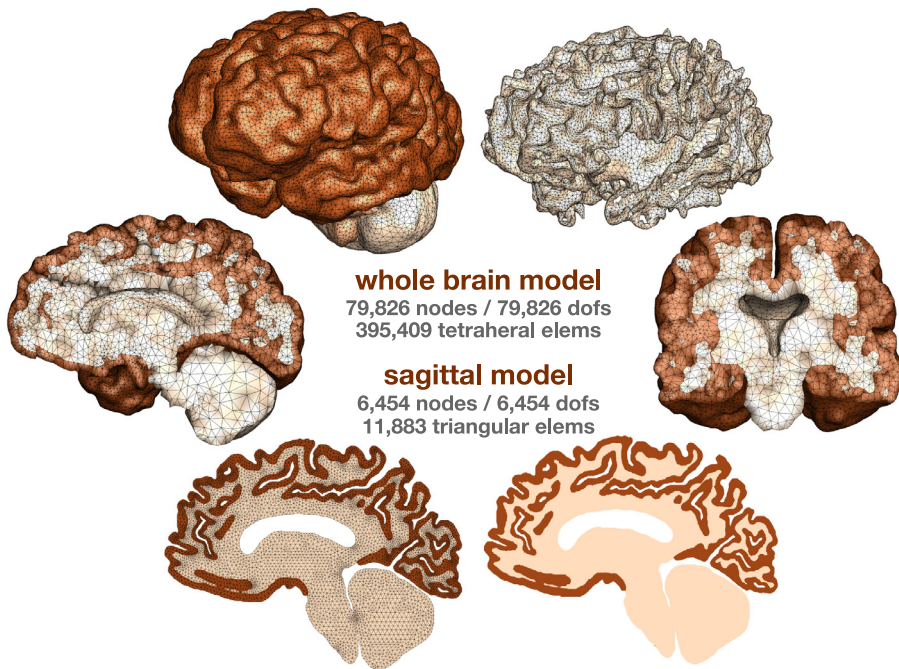


**Fig. 4.** Brain models. Two-dimensional sagittal model and three-dimensional whole brain model with discrete representations of gray and white matter regions created from magnetic resonance images of a healthy human brain.

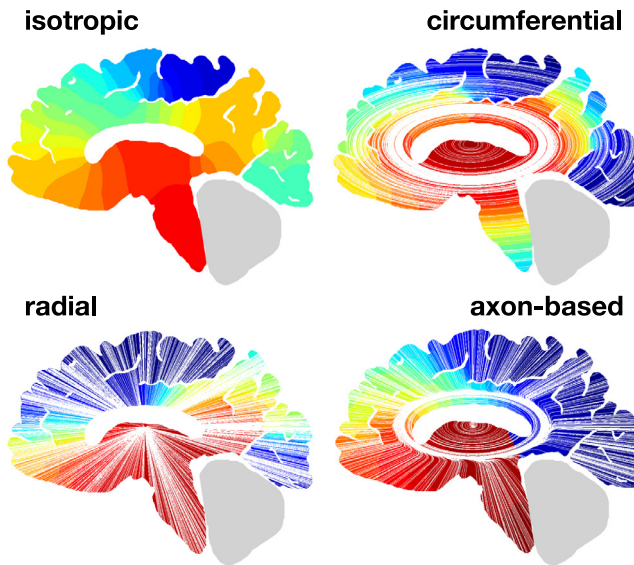


**Fig. 5.** Fiber model for two-dimensional sensitivity analysis. Isotropic sagittal model and anisotropic sagittal models with parameterized circumferential, radial, and axon-based fiber orientations  $\mathbf{n}$  resulting in 11,883 discrete fiber orientations, one for each element.

and axon-based sagittal simulations. In three dimensions, we create a fiber orientation map from diffusion tensor magnetic resonance images of our healthy, 32-year old subject and register the axonal fiber orientation  $\mathbf{n}$  on our whole brain model in Fig. 4. This results in an element-based fiber orientation map with 395,409 discrete fiber orientations  $\mathbf{n}$ , one for each element. Fig. 6 illustrates the sagittal, whole brain, and coronal views of the discrete fiber orientations for our whole brain simulation.

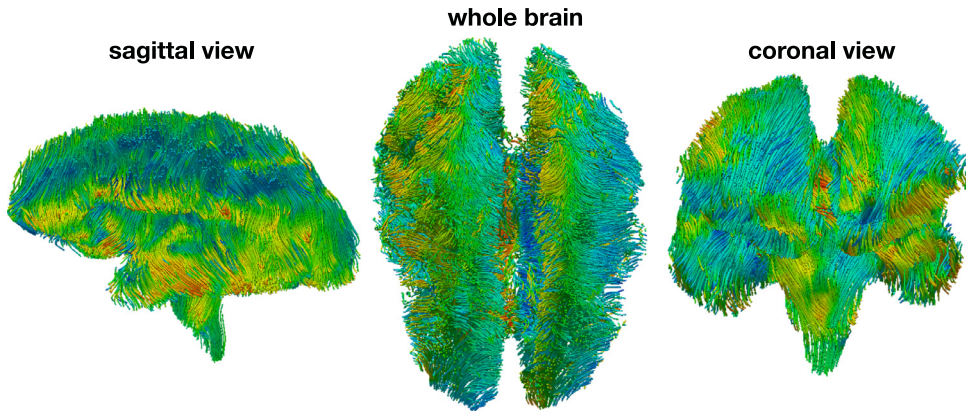


**Fig. 6.** Fiber model for three-dimensional simulations. Sagittal, whole brain, and coronal view of fiber orientations  $\mathbf{n}$  reconstructed from diffusion tensor magnetic resonance images and registered on the three-dimensional brain model resulting in 395,409 discrete fiber orientations, one for each element.

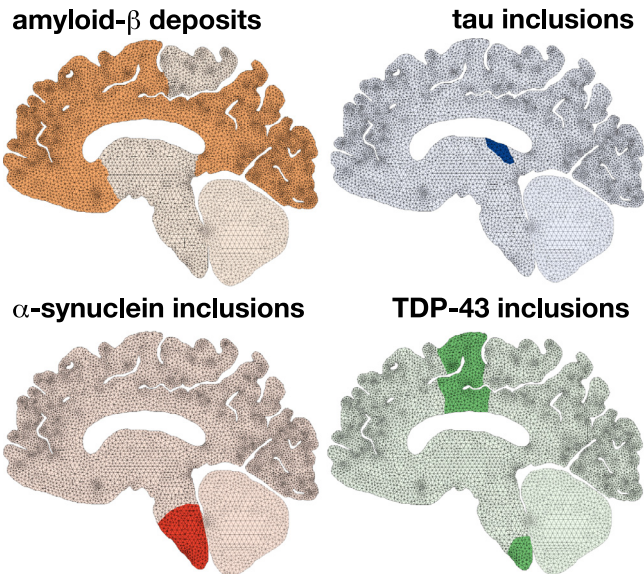


**Fig. 7.** Neurodegeneration models. Initial conditions for simulations of prion-like spreading of amyloid- $\beta$  deposits in Alzheimer's disease, tau inclusions in Alzheimer's disease,  $\alpha$ -synuclein inclusions in Parkinson's disease, and TDP-43 inclusions in amyotrophic lateral sclerosis. The initial concentration of misfolded protein is zero across the brain except for the local seeding regions highlighted in orange, blue, red, and green, where it is slightly elevated.

## 2.7. Neurodegeneration models

Fig. 7 illustrates the seeding of amyloid- $\beta$  deposits in Alzheimer's disease, tau inclusions in Alzheimer's disease,  $\alpha$ -synuclein inclusions in Parkinson's disease, and TDP-43 inclusions in amyotrophic lateral sclerosis. We model seeding of misfolded protein through non-homogeneous initial conditions of the misfolded protein concentration. Initially, the misfolded protein concentration is zero across the brain,  $c_0 = 0$  in  $\mathcal{B} \setminus \mathcal{B}^*$ , except for the local seeding regions  $\mathcal{B}^*$  highlighted in orange, blue, red, and green, where it is slightly elevated,  $c_0 > 0$  in  $\mathcal{B}^*$ . We infer the four different seeding regions from the post-mortem analysis of Alzheimer's, Parkinson's and amyotrophic lateral sclerosis brains (Jucker and Walker, 2013) according to Fig. 1 and map them onto our sagittal model in Fig. 7: Amyloid- $\beta$  deposits in Alzheimer's disease shown in orange first appear in the neocortex (Jucker and Walker, 2011); tau inclusions in Alzheimer's disease shown in blue occur first in the locus caeruleus and transentorhinal layer (Braak and Braak, 1991);  $\alpha$ -synuclein inclusions in Parkinson's disease shown in red first occur in the dorsal motor nucleus and in the anterior olfactory nucleus (Braak et al., 2003); TDP-43 inclusions in amyotrophic lateral sclerosis shown in green develop first in the agranular motor cortex, brainstem motor nuclei of cranial nerves, and spinal cord motorneurons (Brettschneider et al., 2013). We report the neurodegenerative pattern through two different plots, concentration maps and activation maps. Concentration maps illustrate the primary variable, the concentra-

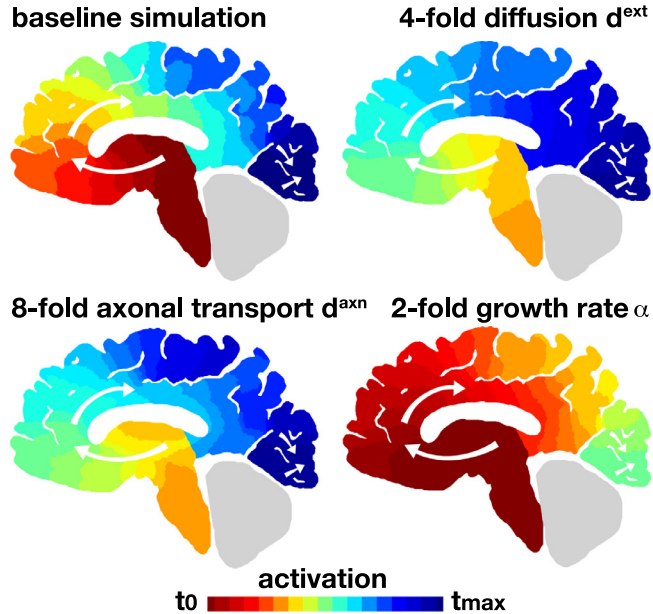


**Fig. 8.** Sensitivity with respect to the extracellular diffusion  $d^{\text{ext}}$ , the axonal transport  $d^{\text{axn}}$ , and the growth rate  $\alpha$ . Prion-like spreading of tau inclusions in Alzheimer's disease with baseline simulation, top left; four-fold increase of extracellular diffusion, top right; eight-fold increase of axonal transport, bottom left; and two-fold increase of growth, bottom right.

tion of misfolded protein  $c(x, t)$ , at every point  $x$  across the domain  $\mathcal{B}$  at a given point in time  $t$ , ranging from  $0.0 \leq c \leq 1.0$ . Concentration maps are common in the physics community as they highlight the spatial evolution of the primary unknown, the concentration  $c$ . Activation maps illustrate the activation time  $t(x)$ , the time at which the local concentration of misfolded protein exceeds a critical value of  $c^{\text{crit}} = 0.95$ . Activation maps are common in the medical community as they highlight the temporal progression of a biomarker above its detection threshold  $c^{\text{crit}}$ . To demonstrate the global evolution of neurodegeneration, we also report the temporal evolution of the biomarker abnormality, the total concentration of misfolded protein integrated across the entire brain,  $C(t) = \int_{\mathcal{B}} c(\mathbf{x}, t) dV$ .

### 3. Results

Our prion-like spreading model in Eqs. (8) and (9) has five parameters that control the pattern formation during neurodegeneration: The growth rate  $\alpha$  characterizes the local increase of the misfolded protein concentration; the extracellular diffusion  $d^{\text{ext}}$  characterizes the isotropic spreading of misfolded protein through the extracellular space, the axonal transport  $d^{\text{axn}}$  characterizes the anisotropic spreading of misfolded protein through intracellular transport, the axonal orientation  $\mathbf{n}$  characterizes the anatomic pathway of fast spreading, and the seeding region  $\mathcal{B}^*$  characterizes the regional onset of neurodegeneration. In this section, we probe the effect of these five parameters in a systematic sensitivity analysis and then perform a simulation of the prion-like spreading of misfolded protein in Alzheimer's disease, Parkinson's disease, and amyotrophic lateral sclerosis.

#### 3.1. Sensitivity analysis with respect to extracellular diffusion, axonal transport, and growth

Fig. 8 illustrates the results of our sensitivity analysis with varying extracellular diffusion  $d^{\text{ext}}$ , axonal transport  $d^{\text{axn}}$ , and growth rate  $\alpha$ . For all four simulations, we assume an axon-based fiber orientation according to Fig. 5, bottom right, with a pronounced elliptical fiber orientation around the ventricle and outward pointing fibers in all other regions. In all four cases, we seed tau inclusions in the locus coeruleus and transentorhinal layer to mimic the characteristic onset of Alzheimer's disease (Braak and Braak, 1991) motivated by the blue graphics in Fig. 1 (Jucker and Walker, 2013) and specified in detail for our sagittal model in Fig. 7. The rainbow color code highlights the activation time, i.e., the time  $t$  at which the regional concentration of misfolded protein exceeds the critical threshold of 95%, thus  $c > 0.95$ . Red regions activate first, blue regions activate last. For the baseline simulation, top left, we choose an extracellular diffusion of  $d^{\text{ext}} = 1.5 \text{ cm}^2/\text{year}$  in both gray and white matter, and an axonal transport of  $d^{\text{axn}} = 3.0 \text{ cm}^2/\text{year}$  in white and  $d^{\text{axn}} = 0.0 \text{ cm}^2/\text{year}$  in gray matter, and a growth rate of  $\alpha = 0.6 / \text{year}$  in white and  $\alpha = 0.3 / \text{year}$  in gray matter. For the sensitivity analysis, we increase the extracellular diffusion by a factor four to  $d^{\text{ext}} = 6.0 \text{ cm}^2/\text{year}$ , top right, the axonal transport by a factor eight

to  $d^{\text{axn}} = 24.0 \text{ cm}^2/\text{year}$ , bottom left, and the growth rate by a factor two to  $\alpha = 1.2 / \text{year}$  in white and  $\alpha = 0.6 / \text{year}$  in gray matter, bottom right, while keeping the other parameters at the baseline values.

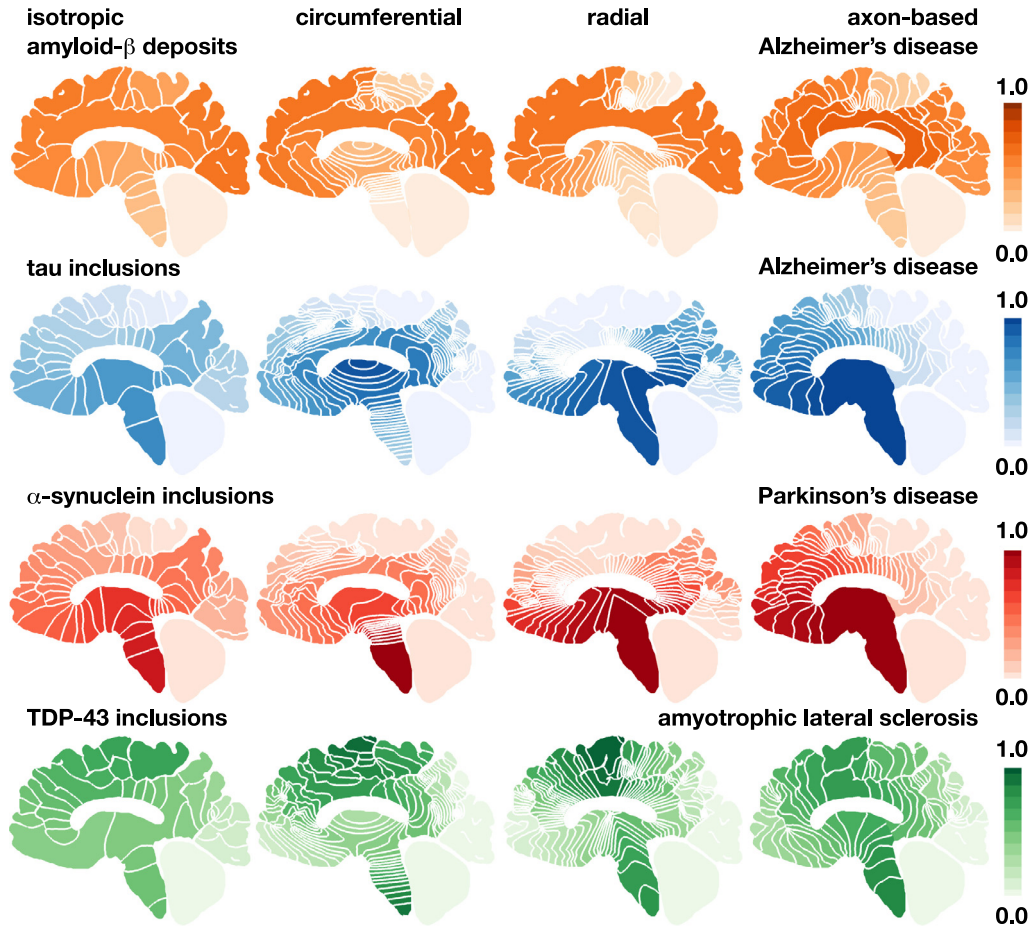
The activation pattern of the baseline simulation agrees well with the characteristic progression of proteinaceous lesions in Alzheimer's disease inferred from post-mortem analysis of diseased brains: Neurofibrillary tau tangles in Alzheimer's disease initiate first in the locus coeruleus and transentorhinal layer, then spread to the transentorhinal region and the proper entorhinal cortex, from where they affect virtually all interconnected neocortical brain regions (Braak and Braak, 1991). The characteristic propagation pattern of our baseline simulation indicated through the white arrows in Fig. 8, top left, matches the clinically observed pattern in Fig. 1. Increasing the growth rate  $\alpha$  triggers a faster increase of the local misfolded protein concentration in the initial seeding region, which causes a faster spreading of pathogenic protein, and reduces the overall activation time, bottom right. Activation starts earlier and finishes faster than in the baseline case. Increasing the extracellular diffusion  $d^{\text{ext}}$  and axonal transport  $d^{\text{axn}}$  causes a faster spreading of misfolded protein out of the initial seeding region, top right and bottom left. Activation starts later but finishes faster than in the baseline case. Misfolded protein accumulates in the brain stem, where it first reaches the critical concentration of 95%. From here, it gradually spreads, first towards the frontal regions and then towards the lateral regions. Increasing the anisotropic diffusion  $d^{\text{axn}}$  with a pronounced fiber orientation  $\mathbf{n}$  around the ventricle causes a faster spreading of misfolded protein around the ventricular region, bottom left, especially compared to the case of increased extracellular diffusion  $d^{\text{ext}}$ , top right. Strikingly, when increasing spreading, either extracellular diffusion  $d^{\text{ext}}$  or axonal transport  $d^{\text{axn}}$ , the initial seeding region no longer coincides with the region that first reaches the critical concentration of 95%. This suggests that a misbalance between growth and spreading can cause a faster outflow of misfolded protein than is locally produced. In combination with homogeneous Neumann boundary conditions that prevent an outflow across the boundary, narrow regions like the brainstem exhibit a rapid local increase of misfolded protein, and can, under certain conditions, even outpace the initial seeding region. Clearly, this effect is caused by the interplay of geometry and boundary conditions that is invisible to the one-dimensional model problem in Fig. 3. Taken together, our sensitivity analysis suggests that the simulated activation pattern is rather insensitive to the growth rate  $\alpha$ , which mainly affects the timing of activation but not the overall pattern, and highly sensitive to both extracellular diffusion  $d^{\text{ext}}$  and axonal transport  $d^{\text{axn}}$ , which affect both the timing of activation and the emerging concentration pattern.

### 3.2. Sensitivity analysis with respect to axonal orientation and seeding region

Fig. 9 illustrates the results of our sensitivity analysis for varying fiber orientations  $\mathbf{n}$  and seeding regions  $B^*$ . The four columns highlight the effect of four different fiber orientations according to Fig. 5, isotropic and anisotropic with pronounced circumferential, radial, and axon-based fiber orientations  $\mathbf{n}$ , from left to right. The four rows illustrate the effect of four different seeding regions  $B^*$  to mimic the prion-like spreading of amyloid- $\beta$  deposits in Alzheimer's disease, tau inclusions in Alzheimer's disease,  $\alpha$ -synuclein inclusions in Parkinson's disease, and TDP-43 inclusions in amyotrophic lateral sclerosis, from top to bottom. The color code highlights the regional distribution of the misfolded protein concentration  $c$ , recorded at the time point, at which the total global concentration has reached 50%, the white lines are the concentration isolines. Isotropic extracellular diffusion alone seems to trigger a homogeneous spreading of misfolded protein across the brain with unphysiological concentration patterns that are almost indistinguishable for all four seeding cases, left column. Circumferential transport generates activation patterns that are elliptically oriented around the ventricle, either from outside in or from inside out, but seem also rather unphysiological. Radial transport activates the brain in rays that radiate outward from the ventricle and triggers radially oriented activation patterns that are also rather unphysiological. Axon-based transport with a pronounced spreading around the ventricles combined with an outward spreading towards the cortex generates distinct activation patterns for all four seeding cases. These activation patterns seem to agree well with the characteristic progression of specific proteinaceous lesions in Alzheimer's disease, Parkinson's disease, and amyotrophic lateral sclerosis (Jucker and Walker, 2013) summarized in Fig. 1. Taken together, our sensitivity analysis suggests that the simulated activation pattern is highly sensitive to both the fiber orientation  $\mathbf{n}$  and initial seeding region  $B^*$ . The importance of anisotropic diffusion along established anatomical pathways suggests that axonal transport of misfolded protein plays a critical role in neurodegeneration. Axonal transport is a characteristic spreading mechanism in prion disease and suggests that neurodegenerative disorders including Alzheimer's disease, Parkinson's disease, and amyotrophic lateral sclerosis are capable of spreading in a prion-like fashion.

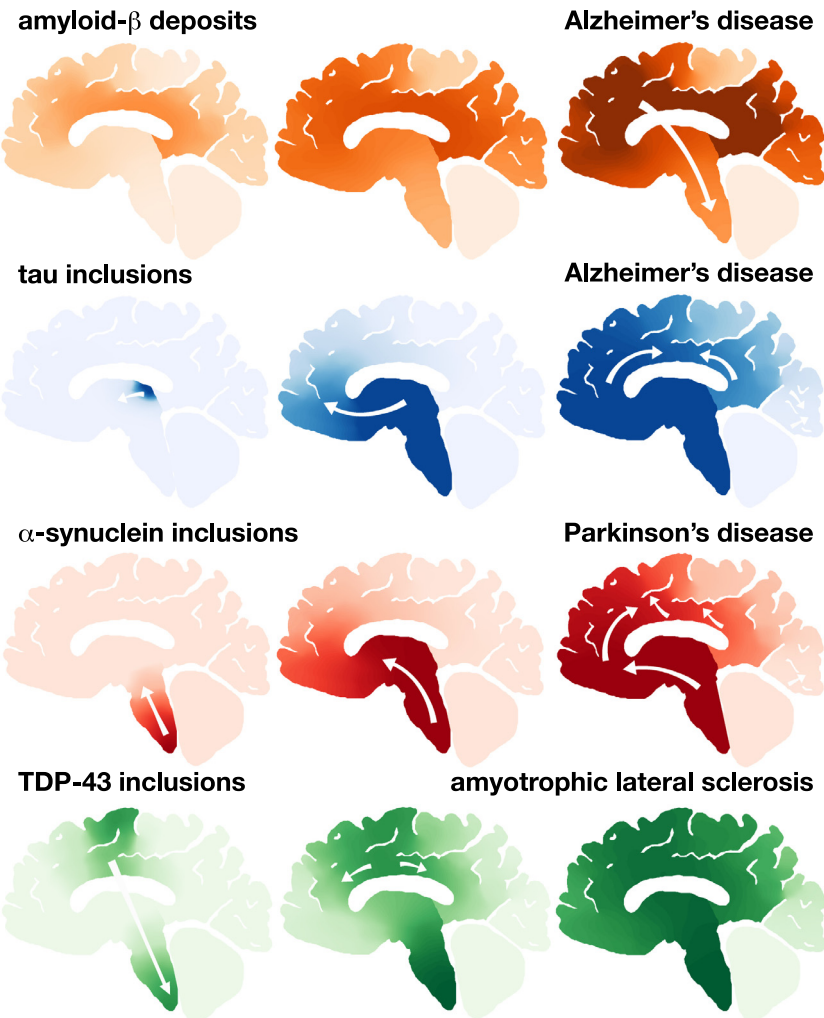
### 3.3. Prion-like spreading in neurodegenerative disease

Fig. 10 summarizes our simulations of prion-like spreading of amyloid- $\beta$  deposits in Alzheimer's disease, tau inclusions in Alzheimer's disease,  $\alpha$ -synuclein inclusions in Parkinson's disease, and TDP-43 inclusions in amyotrophic lateral sclerosis. For these simulations, we used the sagittal model with 6454 nodes and 11,883 triangular elements according to Fig. 4, the axon orientation  $\mathbf{n}$  according to Fig. 5, the initial seeding regions according to Fig. 7, and the baseline material parameters according to Fig. 8, top left, with an extracellular diffusion of  $d^{\text{ext}} = 1.5 \text{ cm}^2/\text{year}$  in both gray and white matter, an axonal transport of  $d^{\text{axn}} = 3.0 \text{ cm}^2/\text{year}$  in white and  $d^{\text{axn}} = 0.0 \text{ cm}^2/\text{year}$  in gray matter, and a growth rate of  $\alpha = 0.6 / \text{year}$  in white and  $\alpha = 0.3 / \text{year}$  in gray matter. In all four cases, we simulated a total time period of  $T = 40$  years, discretized by



**Fig. 9.** Sensitivity with respect to the fiber orientation  $\mathbf{n}$  and initial seeding region. Prion-like spreading of amyloid- $\beta$  deposits in Alzheimer's disease, tau inclusions in Alzheimer's disease,  $\alpha$ -synuclein inclusions in Parkinson's disease, and TDP-43 inclusions in amyotrophic lateral sclerosis, from top to bottom. Simulation of isotropic diffusion, and anisotropic diffusion with circumferential axons, radial axons, and combined circumferential and radial axon orientations inspired by diffusion tensor magnetic resonance imaging, from left to right. The color code indicates the local concentration of misfolded protein, recorded at 50% of the total global concentration; the white lines highlight the concentration isolines.

$n_{\text{step}} = 120$  time steps of  $\Delta t = 1/3$  year. The three columns highlight three stages of progressive neurodegeneration, from left to right, with white arrows indicating the spreading of lesions. The simulations in Fig. 10 display excellent agreement with the characteristic progression of specific proteinaceous lesions in neurodegenerative diseases over time inferred from cross-sectional autopsy studies of human brains (Jucker and Walker, 2013) illustrated in Fig. 1: Amyloid- $\beta$  deposits in Alzheimer's disease shown in orange first appear in the neocortex, followed by the allocortex, and ultimately affect all regions of the subcortex (Thal et al., 2002). Neurofibrillary tau tangles in Alzheimer's disease shown in blue occur first in the locus coeruleus and transentorhinal layer, then spread to the transentorhinal region and the proper entorhinal cortex, frown where they affect virtually all interconnected neocortical brain regions (Braak and Braak, 1991).  $\alpha$ -synuclein inclusions in Parkinson's disease shown in red first occur in the dorsal motor nucleus and in the anterior olfactory nucleus, then expand into the brain stem, and take an upward course to involve the cortex, from the anteromedial temporal mesocortex to the neocortex (Braak et al., 2003). TDP-43 inclusions in amyotrophic lateral sclerosis shown in green develop first in the agranular motor cortex, brainstem motor nuclei of cranial nerves, and spinal cord motorneurons, then affect the prefrontal neocortex and the brainstem, the postcentral neocortex and striatum, and finally the temporal lobe, and the hippocampus (Brettschneider et al., 2013). Figs. 11 and 12 visualize the three-dimensional spreading of misfolded protein across the whole brain. The observed spreading patterns in Fig. 11 confirm the two-dimensional simulations in Fig. 10 and agree well with the patterns observed in cross-sectional autopsy studies of human brains reported above (Jucker and Walker, 2013) and summarized in a recent review (Goedert et al., 2017). The sagittal, transverse, and coronal sections and the whole brain in Fig. 12 complete our picture of the overall concentration pattern throughout the entire brain. Taken together, our simulations suggest that the Fisher–Kolmogorov Eq. (8) in combination with the anisotropic diffusion Eq. (9) can successfully predict the emerging two- and three-dimensional patterns of misfolded protein concentrations across the brain. The Fisher–Kolmogorov equation is a



**Fig. 10.** Prion-like spreading across sagittal section. Amyloid- $\beta$  deposits in Alzheimer's disease; tau inclusions in Alzheimer's disease;  $\alpha$ -synuclein inclusions in Parkinson's disease; and TDP-43 inclusions in amyotrophic lateral sclerosis. Three stages of progressive neurodegeneration, from left to right, with white arrows indicating the putative spread of the lesions. Simulations display excellent agreement with the characteristic progression of specific proteinaceous lesions in neurodegenerative diseases over time inferred from post-mortem analyses of brains (Jucker and Walker, 2013) in Fig. 1.

nonlinear equation that is highly sensitive to its material parameters. Our simulations demonstrate that the success of the simulation critically depends on the right balance between extracellular diffusion  $d^{\text{ext}}$ , axonal transport  $d^{\text{axn}}$ , and growth  $\alpha$ , the anatomically correct modeling of the axonal orientation  $\mathbf{n}$ , and the selection of the appropriate seeding region  $B^*$ .

### 3.4. Biomarker abnormality in neurodegenerative disease

Fig. 13 summarizes the global biomarker abnormality as a result of the prion-like spreading of amyloid- $\beta$  deposits, TDP-43 inclusions, tau inclusions, and  $\alpha$ -synuclein inclusions across the sagittal section, left, and across the whole brain, right. The left sagittal curves are an integral representation of the results in Fig. 11 and the right whole brain curves are an integral representation of the results in Figs. 12 and 13. For all four degenerative activation patterns, at each discrete time point  $t$ , we integrate the concentration of misfolded protein across the sagittal section,  $C = \int_B c(\mathbf{x}, t) dA$ , or across the entire brain,  $C = \int_B c(\mathbf{x}, t) dV$ , and map the temporal evolution of the global biomarker abnormality  $C$  across the total time interval of  $T=40$  years. All eight biomarkers follow a similar smooth sigmoidal form which agrees well with classical clinical biomarker models for neurodegeneration (Jack et al., 2010) and with clinical observations (Caroli and Frisoni, 2010). Interestingly, without any further parameter tuning, the two- and three-dimensional curves display a similar sequence with amyloid- $\beta$  spreading the fastest, followed by TDP-43, tau, and  $\alpha$ -synuclein. This agrees with our common understanding that, in Alzheimer's disease, amyloid- $\beta$  becomes abnormal first, followed by tau (Jucker and Walker, 2013). In all eight cases, activation is slow in the first five to ten years after initial seeding, but then increases notably for another ten years, and peaks approximately 20 years after the first occurrence of misfolded protein (Jack and Holtzman, 2013). This agrees well with the common un-

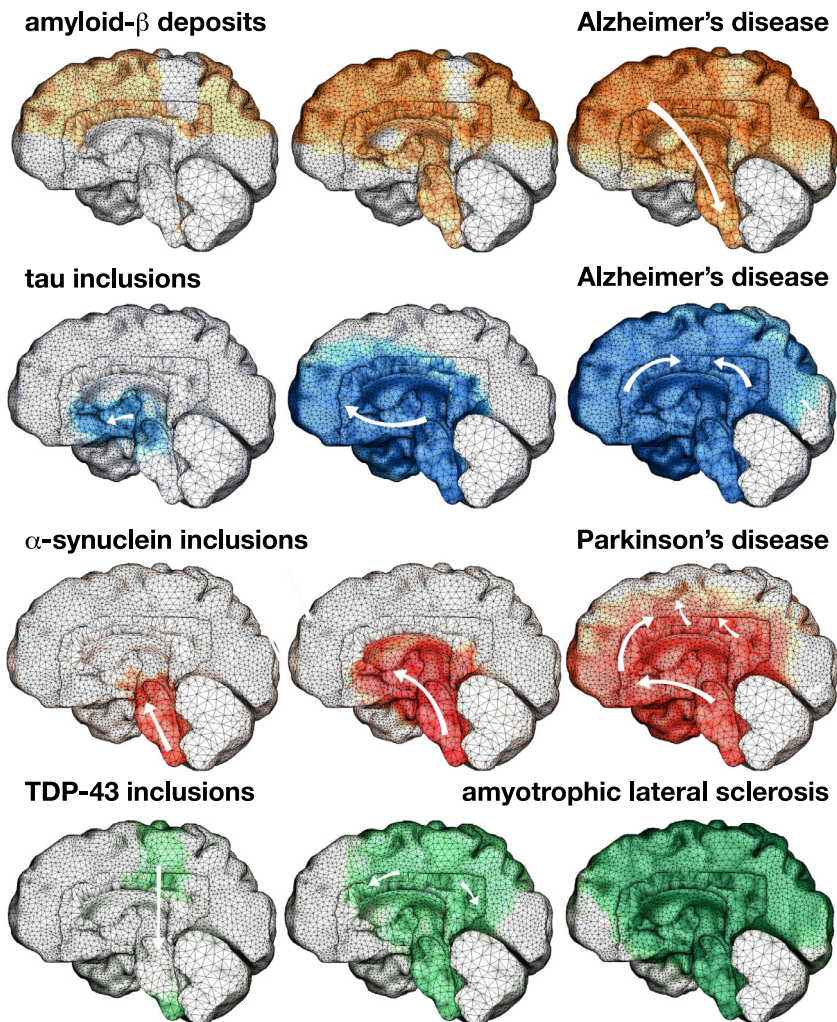


**Fig. 11.** Prion-like spreading across the whole brain visualized in sagittal sections. Amyloid- $\beta$  deposits in Alzheimer's disease; tau inclusions in Alzheimer's disease;  $\alpha$ -synuclein inclusions in Parkinson's disease; and TDP-43 inclusions in amyotrophic lateral sclerosis. Three stages of progressive neurodegeneration, from left to right, with white arrows indicating the spread of the lesions. Simulations display excellent agreement with the characteristic progression of specific proteinaceous lesions in neurodegenerative diseases over time inferred from post-mortem analyses of brains (Jucker and Walker, 2013) in Fig. 1 and with the predictions of the sagittal model in Fig. 10.

derstanding of neurodegeneration (van den Bedem and Kuhl, 2017), in which the disease is characterized by an extremely long, clinically silent, and precisely reproducible incubation period during which the disease amplifies—first locally and then globally throughout the entire brain—followed by a brief and invariably fatal clinical disease (Walker and Jucker, 2015). The time period of 20 years from first initiation to full impairment agrees with the time period of amyloid- $\beta$  detection in Alzheimer's disease (Villemagne et al., 2013), which follows a similar sigmoidal curve (Frisoni et al., 2010). Taken together, our physics-based reaction-diffusion model accurately predicts characteristic local activation patterns in space and global biomarker abnormalities in time. Both our two-dimensional sagittal model and our three-dimensional whole brain model can predict the spatio-temporal evolution of the concentration of misfolded protein in Alzheimer's disease, Parkinson's disease, and amyotrophic lateral sclerosis.

#### 4. Discussion

##### 4.1. Physics-based modeling can predict emerging patterns of neurodegeneration

Various forms of neurodegenerative diseases are associated with misfolded protein in the brain. The objective of this study was to identify common features of neurodegeneration using physics-based modeling and computational simulation. To model emergent patterns in Alzheimer's disease, Parkinson's disease, and amyotrophic lateral sclerosis, we adopt the classical Fisher-Kolmogorov equation (Fisher, 1937), a widely used partial differential equation for population dynamics. We

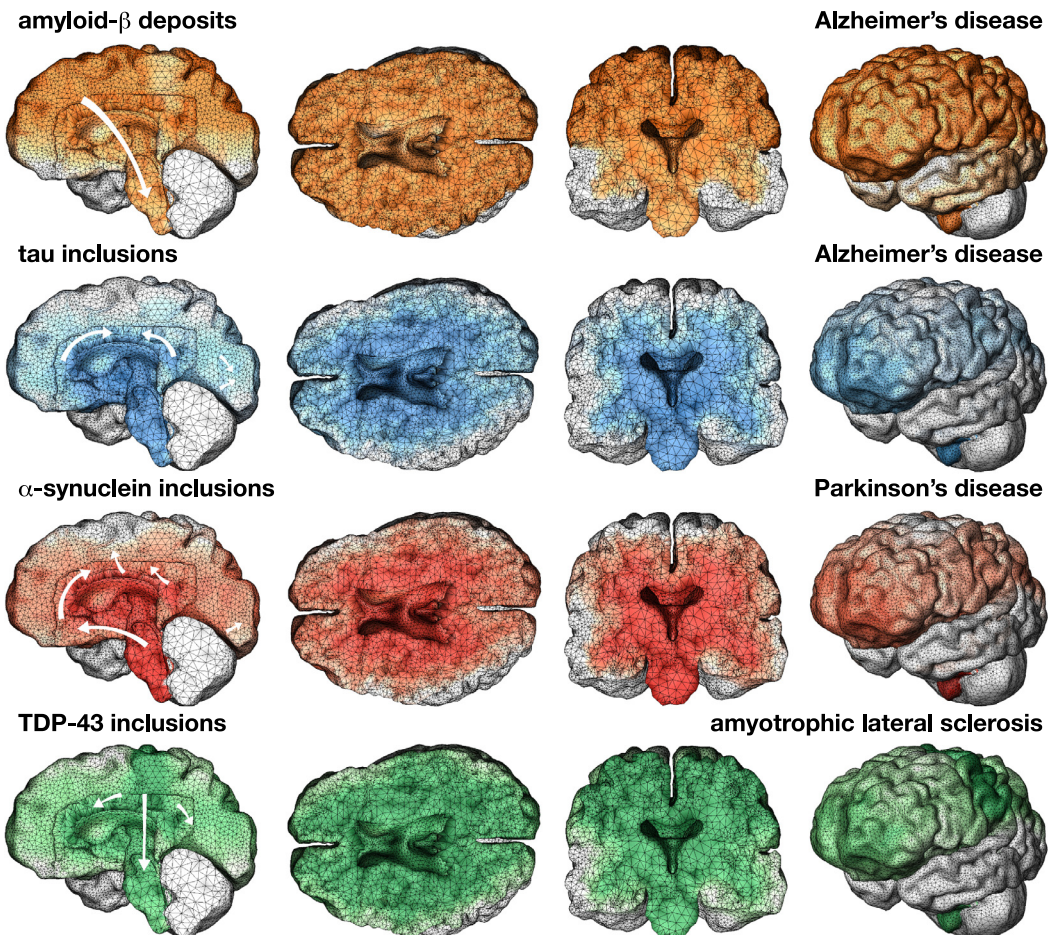


**Fig. 12.** Prion-like spreading across the whole brain visualized in sagittal, transverse, and coronal sections and across the whole brain. Amyloid- $\beta$  deposits in Alzheimer's disease; tau inclusions in Alzheimer's disease;  $\alpha$ -synuclein inclusions in Parkinson's disease; and TDP-43 inclusions in amyotrophic lateral sclerosis.

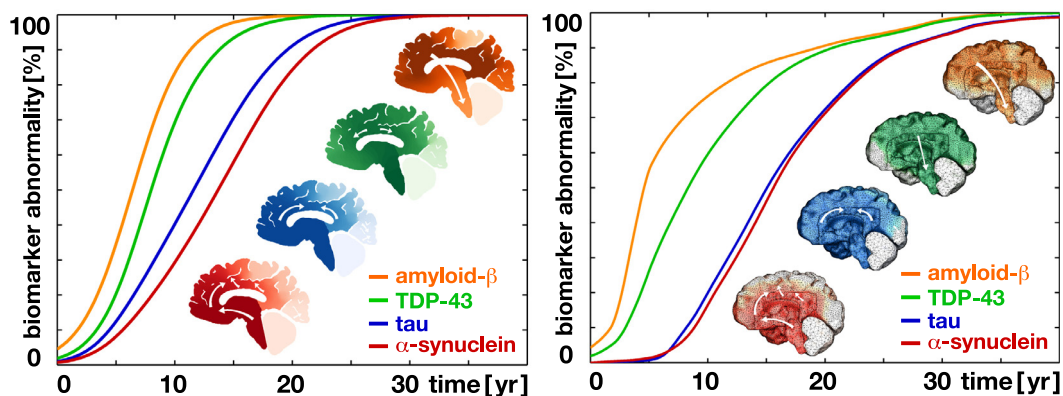


**Fig. 13.** Biomarker abnormality from prion-like spreading of amyloid- $\beta$  deposits, TDP-43 inclusions, tau inclusions, and  $\alpha$ -synuclein inclusions across a sagittal section, left, and across the whole brain, right. The two-dimensional model, left, and three-dimensional model, right, predict similar activation sequences. All eight biomarker-time relations display a smooth sigmoidal form, which is in excellent agreement with clinical biomarker models of neurodegeneration (Jack and Holtzman, 2013).

discretize it in time using finite differences and in space using finite elements, and solve the resulting residual equation using a classical Newton Raphson scheme. Our algorithm generates misfolded protein concentration maps and activation maps, robustly and stably, on arbitrary geometries, from an initial seeding of misfolded protein.

Our one-dimensional model problem in Fig. 3 suggests that the Fisher–Kolmogorov Eq. (8) accurately captures the characteristic features of prion-like diseases: (i) disease progression is inevitable after inoculation and the misfolded protein concentration inevitably converges towards saturation at  $c = 1.0$  once misfolding is seeded with  $c_0 > 0.0$  anywhere in the domain; (ii) the duration of the incubation period depends on both the initial seeding concentration  $c_0$  and the growth rate  $\alpha$ ; and (iii) disease progression is characterized by a long, clinically silent incubation period,  $0.0 < c < c^{\text{crit}}$ , during which the disease gradually amplifies locally, followed by a rapid local increase towards  $c = 1.0$ , and a global spreading from the initial seeding region across the entire domain (Jucker and Walker, 2013).

The Fisher–Kolmogorov equation is a non-linear equation that models the growth and spreading of misfolded protein concentrations (Fisher, 1937). Like any non-linear equation, it is highly sensitive to its material parameters. Since it has never before been used to model neurodegeneration, the values of its parameters remain largely unknown. To identify the relative importance of the individual parameters, we perform a systematic sensitivity analysis and explore the roles of the external diffusion  $d^{\text{ext}}$ , axonal transport  $d^{\text{axn}}$ , growth  $\alpha$ , axonal fiber orientation  $\mathbf{n}$ , and initial seeding region  $B^*$ . Using the simple prion kinetics from Section 2.1, we conclude that, through the growth rate  $\alpha = k_{12}k_0/k_1 - \tilde{k}_1$ , the simulations directly depend on the conversion rate  $k_{12}$  from the healthy to the misfolded conformation, on the equilibrium concentration of healthy protein  $p_0 = k_0/k_1$ , and on the clearance rate  $\tilde{k}_1$ . Our simulations in Fig. 8 suggest that the activation pattern is rather insensitive to the growth rate  $\alpha$ , which mainly affects the timing of activation but not the overall pattern, and highly sensitive to both extracellular diffusion  $d^{\text{ext}}$  and axonal transport  $d^{\text{axn}}$ , which affect both timing and patterning. Our results in Fig. 9 show that an appropriate axonal fiber orientation  $\mathbf{n}$  and an anatomically correct seeding region  $B^*$  are critical to accurately predict the clinically observed concentration profiles.

Once calibrated appropriately, we can use the Fisher–Kolmogorov equation with one and the same parameter set to predict the prion-like spreading of amyloid- $\beta$  deposits in Alzheimer's disease (Thal et al., 2002), tau inclusions in Alzheimer's disease (Braak and Braak, 1991),  $\alpha$ -synuclein inclusions in Parkinson's disease (Braak et al., 2003), and TDP-43 inclusions in amyotrophic lateral sclerosis (Brettschneider et al., 2013). The misfolded protein concentrations of our two-dimensional simulations across a sagittal section in Fig. 10 and our three-dimensional simulations across the whole brain in Figs. 11 and 12 agree well with the characteristic progression of specific proteinaceous lesions in neurodegenerative diseases inferred from post-mortem analyses (Jucker and Walker, 2013) in Fig. 1. When integrated in space and time, our predicted misfolded protein concentrations result in biomarker abnormality curves in Fig. 13 that agree well with clinical biomarker models in neurodegeneration, both qualitatively (Jack and Holtzman, 2013) and quantitatively (Frisoni et al., 2010). We conclude that reaction-diffusion equations of the Fisher Kolmogorov type, combined with anisotropic diffusion, are well suited to predict the prion-like features of growth and spreading, both in space and time, in various neurodegenerative diseases.

#### 4.2. Misfolded proteins spread across the brain by extracellular diffusion and axonal transport

A defining feature of prion-like disease is the spreading of misfolded protein from an initial seeding region across the entire brain (Hall and Patuto, 2012). There is general agreement that two distinct mechanisms are responsible for this spreading, extracellular diffusion and axonal transport. In the clinical literature, diffusion is typically associated with neuronal proximity (Frost et al., 2009) and axonal transport with neuronal connectivity (Seeley et al., 2009). Here we adopt an anisotropic diffusion Eq. (9) and model extracellular diffusion or neuronal proximity as isotropic diffusion and axonal transport or neuronal connectivity as anisotropic diffusion along a characteristic anatomical direction. A similar approach has recently been proposed to model the anisotropic diffusion of glioma invasion (Painter and Hillen, 2013) and brain tumor spreading (Swan et al., 2018) with preferred spreading directions from diffusion tensor magnetic resonance imaging.

While intracellular transport is relatively well understood, the underlying mechanisms of intercellular transport are far less clear. Throughout the past decade, numerous research groups have performed in vitro and in vivo studies to better understand the neuronal uptake, transport, and release of misfolded protein (Jucker and Walker, 2018). Of the four proteins simulated here, amyloid- $\beta$  is probably the most extensively studied. Studies have found that injecting amyloid- $\beta$  extracts into a specific brain region triggers amyloid- $\beta$  deposits in remote axonally connected regions (Jucker and Walker, 2011). However, because amyloid- $\beta$  pathology is primarily extracellular, its propagation does not necessarily explain the spread of neurodegeneration by cell-to-cell transport (Holmes and Diamond, 2014). Tau, in contrast, is considered an intracellular protein, at least under healthy conditions. Under diseased conditions, the occurrence of misfolded tau in the extracellular space is a classical hallmark of neurodegeneration (Hardy and Revesz, 2012). In vitro studies have demonstrated the uptake of misfolded tau protein via endocytosis by cultured cells where it induced misfolding and aggregation of initially healthy endocytosis tau (Frost et al., 2009). For  $\alpha$ -synuclein, in vivo studies have demonstrated cell-to-cell transfer of human  $\alpha$ -synuclein from transgenic mice into implanted wild-type mouse neural stem cells (Desplats et al., 2009).

Several studies have argued that the relatively stereotyped propagation patterns in neurodegeneration support the hypothesis of axonal transport as the major mechanism in the spread of proteopathic seeds (Jucker and Walker, 2013). Yet, the precise roles of neuronal proximity and connectivity remain unknown (Seeley et al., 2009). Our physics-based model of prion-like spreading allows us to virtually probe the relative importance of both phenomena, simply by varying the aspect ratio between the coefficients of extracellular diffusion  $d^{\text{ext}}$  and axonal transport  $d^{\text{axn}}$ . Our sensitivity analysis in Fig. 8 sug-

gests that an extracellular-to-intracellular diffusion ratio of 1:2 of our baseline model predicts a prion-like spreading of tau inclusions that agrees well with the clinical picture in Alzheimer's disease in Fig. 1. Increasing and decreasing this aspect ratio to 2:1 and 1:16 generates non-pathological activation patterns, either dominated by a too regular isotropic diffusion or by a too irregular anisotropic diffusion. Our direct comparison of isotropic and anisotropic diffusion for all four pathologies in Fig. 10 confirms this observation and substantiates the notion of a faster transport along specific directions (Guo et al., 2017). The resulting anisotropic diffusion patterns mimic the pathologically observed trafficking of proteopathic seeds amongst interconnected brain regions in Fig. 1. This suggests that comprehensive pathogenesis models should include both, misfolded protein aggregation and selective, network-driven neuronal vulnerability (Seeley et al., 2009). While there is a general agreement on the stereotypic two-dimensional activation patterns across sagittal sections (Jucker and Walker, 2013; Walker and Jucker, 2015), much less is known about the activation patterns across transverse or coronal sections, or across the three-dimensional brain as a whole. More detailed knowledge about these activation patterns would be needed to rigorously validate three-dimensional whole brain simulations. A better understanding of the spreading of misfolded protein and the underlying mechanisms of its cellular uptake, transport, and release (Walker and LeVine, 2012) could open new therapeutic opportunities towards blocking misfolded protein uptake and promoting its clearance using antibodies or small molecules (Holmes and Diamond, 2014).

#### 4.3. Our predicted biomarkers from prion-like spreading agree well with empirical biomarker models

Neurodegenerative diseases are slowly progressing disorders in which pathophysiological abnormalities precede clinical symptoms, often by at least a decade or two (Villemagne et al., 2013). Biomarkers are physiological, biochemical, or anatomic characteristics that can be objectively measured to quantify a normal biological process, a pathogenic process, or a pharmacological response to a therapeutic intervention (Shaw et al., 2007). In neurodegenerative disorders, biomarkers do not occur simultaneously, but typically follow a specific temporal sequence. Biomarker models describe both the temporal sequence of individual biomarkers and their functional evolution in time (Jack et al., 2010). For example, in Alzheimer's disease, it is now well accepted that biomarkers associated with amyloid- $\beta$  become abnormal first, followed by tau, brain atrophy, and cognitive impairment (Jack and Holtzman, 2013). Interestingly, without parameter tuning, both our two- and three-dimensional models in Fig. 13 predict noticeable biomarker abnormalities in amyloid- $\beta$  about five to ten years before they develop biomarker abnormalities in tau which agrees well with these clinical observations. To simulate not only amyloid- $\beta$  and tau, but also brain atrophy (Frisoni et al., 2010), we have recently linked our biochemical model for neurodegeneration to a biomechanical model for whole brain atrophy (Weickenmeier et al., 2018). We have simulated atrophy profiles across the brain to explore the relation between gray and white matter atrophy (Harris et al., 2018), and plan to couple these biomechanics models to our predicted misfolded tau concentrations.

To characterize individual biomarkers in time, sigmoid models have been proposed for the general shape or functional form of biomarker evolution (Jack et al., 2010). In our model, biomarker curves naturally result from integrating the total concentration of misfolded protein across the entire brain,  $C(t) = \int_B c(\mathbf{x}, t) dV$ . Notably, all our eight biomarker curves in Fig. 13 inherently capture the proposed sigmoid shape with an initially silent undetectable regime of five to ten years, a rapid increase for another ten years, and a plateau after twenty years of initial seeding (Jack and Holtzman, 2013). This excellent agreement with empirical biomarker models suggests that the Fisher–Kolmogorov Eq. (8) is well-suited to capture the characteristic time line of individual biomarkers in various types of neurodegeneration.

Initial biomarker models were purely empirical, and although they have been progressively refined, most models remain qualitative in nature. To validate the proposed sigmoid shape, a recent study compared amyloid- $\beta$ , tau, and atrophy-based biomarkers of 576 brains throughout three years, fitted the sigmoid parameters, and confirmed that sigmoid models generally provide a better fit than linear models (Caroli and Frisoni, 2010). Another study quantified the rates of amyloid- $\beta$  deposition in 200 individuals throughout four years and found that the time period of amyloid- $\beta$  deposition extended more than two decades (Villemagne et al., 2013). These findings agree both qualitatively and quantitatively with our simulated amyloid- $\beta$  abnormalities in Fig. 13. A more sophisticated approach applied an epidemic spreading model to simulate amyloid- $\beta$  concentrations and compared them against amyloid- $\beta$  datasets of 733 healthy and neurodegenerative brains (Iturria-Medina et al., 2014). In contrast to the model proposed here, this work focused more on network-type patterning rather than on neurodegenerative patterns across the entire brain. While biomarker modeling is increasingly recognized as both important and insightful, existing models remain phenomenological and their parameters lack a clear pathophysiological interpretation. A natural next step would be to better correlate growth and spreading to the underlying kinetics of protein recruitment  $k_{11'}$ , misfolding  $k_{1'2'}$ , and fragmentation  $k_{2'2}$  in Fig. 2, for example via refining our kinetic model of prion-like spreading in Section 2.1 (Pöschel et al., 2003), to provide a more mechanistic interpretation of our model parameters (Masel et al., 1999).

Fortunately, the accumulation of misfolded protein precedes changes in brain volume and cognition by one or two decades and the rate of accumulation is slow. This opens a wide time window of opportunity for possible intervention. Identifying reliable predictive indicators of neurodegeneration would enable early intervention, for example in the form of antibody treatment, ideally when the individual is still at an asymptomatic stage. A better understanding of the sequence of biomarkers and their temporal evolution, similar to Fig. 13, would allow us to establish a prognostic timeframe of disease progression. This could have important fundamental and clinical implications: From a scientific perspective, it could inform the design of therapeutic trials and identify the most informative time points for data collection; from an economic

perspective, it could provide important insights to accurately estimate the socioeconomic burden of neurodegeneration; and from a clinical perspective, it could help identify the most effective time periods for pharmacological intervention.

## 5. Conclusion

The prion hypothesis is a unifying concept that explains the growth and spreading of neurodegenerative disorders via the seeded corruption of misfolded proteins. While the general idea of identifying common principles of neurodegeneration is intriguing, adopting the prion paradigm to explain the pathology of neurodegenerative disorders remains controversial. Rather than engaging in this biochemistry-based discussion, the objective of this study was to identify unified principles of a variety of neurodegenerative disorders via physics-based modeling. Our study suggests that the simplest possible mechanism for the growth and spreading of misfolded protein is nonlinear reaction combined with anisotropic diffusion. We show that the stereotypic patterns of amyloid- $\beta$  deposits, tau inclusions,  $\alpha$ -synuclein inclusions, and TDP-43 inclusions evolve according to a Fisher–Kolmogorov-type equation and spread across the brain via extracellular diffusion and axonal transport. To identify the relative roles of extracellular diffusion and axonal transport, we perform a systematic sensitivity analysis and conclude that intracellular spreading within an anatomically well-defined axonal network is a common underlying principle in neurodegenerative disease. Strikingly, our simple reaction-diffusion model with one and the same set of parameters predicts misfolded protein concentrations and biomarker abnormalities that agree both qualitatively and quantitatively with the histological observations and biomarker profiles in Alzheimer's disease, Parkinson's disease, and amyotrophic lateral sclerosis. Understanding the common mechanisms of growth and spreading of misfolded proteins is important for the design of predictive biomarkers and therapeutic targets towards increasing treatment outcomes in various types of age-related neurodegenerative disorders.

## Acknowledgments

This study was supported by the Bio-X IIP seed grant 'Molecular Mechanisms of Chronic Traumatic Encephalopathy', the Engineering and Physical Sciences Research Council grant EP/R020205/1, and the NSF grant CMMI 1727268 'Understanding Neurodegeneration across the Scales'.

## Supplementary material

Supplementary material associated with this article can be found, in the online version, at doi:[10.1016/j.jmps.2018.10.013](https://doi.org/10.1016/j.jmps.2018.10.013).

## References

- Aguzzini, A., Montrasio, F., Kaeser, P.S., 2001. Prions: Health scare and biological challenge. *Nat. Rev. Mol. Cell Biol.* 2, 118–126.
- van den Bedem, H., Kuhl, E., 2017. Molecular mechanisms of chronic traumatic encephalopathy. *Current Opin. Biomed. Eng.* 1, 23–30.
- Braak, H., Braak, E., 1991. Neuropathological staging of Alzheimer-related changes. *Acta Neuropathologica* 82, 239–259.
- Braak, H., Del Tredici, K., Rüb, U., de Vos, R.A.I., Jansen Steur, E.N.H., Braak, E., 2003. Staging of brain pathology related to sporadic Parkinson's disease. *Neurobiol. Aging* 24, 197–211.
- Bretttschneider, J., Tredici, K.D., Toledo, J.B., Robinson, J.L., Irwin, D.J., Grossman, M., Suh, E.R., Van Deerlin, V.M., Wood, E.M., Baek, Y., Kwong, L., Lee, E.B., Elman, L., McCluskey, L., Fang, L., Feldengut, S., Ludolph, A.C., Lee, V.M.Y., Braak, H., Trojanowski, J.Q., 2013. Stages of pTDP-43 pathology in amyotrophic lateral sclerosis. *Ann. Neurol.* 74, 20–38.
- Caroli, A., Frisoni, G.B., 2010. The dynamics of Alzheimer's disease biomarkers in the Alzheimer's disease neuroimaging initiative cohort. *Neurobiol. Aging* 31, 1263–1274.
- Cohen, F.E., Pan, K.M., Huang, Z., Baldwin, M., Fletterick, R.J., Prusiner, S.B., 1994. Structural cues to prion replication. *Science* 264, 530–531.
- Desplats, P., Lee, J., Bae, E.J., Patrick, C., Rockenstein, E., Crews, L., Spencer, B., Masliah, E., Lee, S.J., 2009. Inclusion formation and neuronal cell death through neuron-to-neuron transmission of  $\alpha$ -synuclein. *Proc. Natl. Acad. Sci.* 106, 13010–13015.
- Eigen, M., 1996. Prionics or the kinetic basis of prion diseases. *Biophys. Chem.* 63, A1–A18.
- Fisher, R.A., 1937. The wave of advance of advantageous genes. *Ann. Eugen.* 7, 355–369.
- Frisoni, G.B., Fox, N.C., Jack, C.R., Scheltens, P., Thompson, P.M., 2010. The clinical use of structural MRI in Alzheimer disease. *Nat. Rev. Neurol.* 6, 67–77.
- Frost, B., Jacks, R.L., Diamond, M.J., 2009. Propagation of tau misfolding from the outside to the inside of a cell. *J. Biol. Chem.* 284, 12845–12852.
- Goedert, M., Masuda-Suzukake, M., Falcon, B., 2017. Like prions: the propagation of aggregated tau and  $\alpha$ -synuclein in neurodegeneration. *Brain* 140, 266–278.
- Goriely, A., Geers, M.G.D., Holzapfel, G.A., Jayamohan, J., Jerusalem, A., Sivaloganathan, S., Squier, W., van Dommelen, J.A.W., Waters, S., Kuhl, E., 2015. Mechanics of the brain: perspectives, challenges, and opportunities. *Biomech. Model. Mechanobiol.* 14, 931–965.
- Guo, T., Noble, W., Hanger, D.P., 2017. Roles of tau protein in health and disease. *Acta Neuropathologica* 133, 665–704.
- Hall, G.F., Patuto, B.A., 2012. Is tau ready for admission to the prion club? *Prion* 6, 223–233.
- Hardy, J., Revesz, T., 2012. The spread of neurodegenerative disease. *New England J. Med.* 366, 22.
- Harris, T.C., de Rooij, R., Kuhl, E., 2018. The shrinking brain: Cerebral atrophy following traumatic brain injury. *Ann. Biomed. Eng.* doi:[10.1007/s10439-018-02148-2](https://doi.org/10.1007/s10439-018-02148-2).
- Holmes, B.B., Diamond, M.J., 2014. Prion-like properties of tau protein: the importance of extracellular tau as therapeutic target. *J. Biol. Chem.* 289, 19855–19861.
- Iturria-Medina, Y., Sotero, R.C., Toussaint, P.J., Evans, A.C., 2014. Epidemic spreading model to characterize misfolded proteins propagation in aging and associated neurodegenerative disorders. *PLOS Comput. Biol.* 10, e1003956.
- Jack, C.R., Holtzman, D.M., 2013. Biomarker modeling of Alzheimer's disease. *Neuron* 80, 1347–1358.
- Jack, C.R., Knopman, D.S., Jagust, W.J., Shaw, L.M., Aisen, P.S., Weiner, M.W., Petersen, R.C., Trojanowski, J.Q., 2010. Hypothetical model of dynamic biomarkers of the Alzheimer's pathological cascade. *Lancet Neurol.* 9, 119–128.
- Jarrett, J.T., Lansbury, P.T., 1993. Seeding "one-dimensional crystallization" of amyloid: a pathogenic mechanism in Alzheimer's disease and scrapie? *Cell* 73, 1055–1058.
- Jucker, M., Walker, L.C., 2011. Pathological protein seeding in Alzheimer disease and other neurodegenerative disorders. *Ann. Neurol.* 70, 532–540.

- Jucker, M., Walker, L.C., 2013. Self-propagation of pathogenic protein aggregates in neurodegenerative diseases. *Nature* 501, 45–51.
- Jucker, M., Walker, L.C., 2018. Propagation and spread of pathogenic protein assemblies in neurodegenerative diseases. *Nature Neurosci.* 21, 1341–1349.
- Kolmogorov, A.N., Petrovsky, I.G., Piskunov, N.S., 1937. Investigation of the equation of diffusion combined with increasing of the substance and its application to a biology problem. *Bull. Moscow State Univ. Ser. A* 1, 1–25.
- Masel, J., Jansen, V.A.A., Nowak, M.A., 1999. Quantifying the kinetic parameters of prion replication. *Biophys. Chem.* 77, 139–152.
- Murray, J.D., 2002. Mathematical Biology. I. An Introduction, third edition Springer-Verlag, Berlin Heidelberg.
- Painter, K.J., Hillen, T., 2013. Mathematical modelling of glioma growth: The use of diffusion tensor imaging (DTI) data to predict the anisotropic pathways of cancer invasion. *J. Theor. Biol.* 323, 25–39.
- Pöschel, T., Brilliantov, H.V., Frömmel, C., 2003. Kinetics of prion growth. *Biophys. J.* 85, 3460–3474.
- Prusiner, S.B., 1998. Prions. nobel lecture. *Proc. Natl. Acad. Sci.* 95, 13363–13383.
- Scheckel, C., Aguzzi, A., 2018. Prions, prionoids and protein misfolding disorders. *Nat. Rev. Genet.* 19, 405–418.
- Seeley, W.W., Crawford, R.K., Zhou, J., Miller, B.L., Greicius, M.D., 2009. Neurodegenerative diseases target large-scale human brain networks. *Neuron* 62, 42–52.
- Shaw, L.M., Korecka, M., Clark, C.M., Lee, V.M.Y., Trojanowski, J.Q., 2007. Biomarkers of neurodegeneration for diagnosis and monitoring therapeutics. *Nat. Rev. Drug Disc.* 6, 295–303.
- Stopachinski, B.E., Diamond, M.I., 2017. The prion model for progression and diversity of neurodegenerative diseases. *Lancet Neurol.* 16, 323–332.
- Swan, A., Hillen, T., Bowman, J.C., Murtha, A.D., 2018. A patient-specific anisotropic diffusion model for brain tumor spread. *Bull. Math. Biol.* 80, 1259–1291.
- Thal, D.R., Rub, U., Orantes, M., Braak, H., 2002. Phases of a beta-deposition in the human brain and its relevance for the development of AD. *Neurology* 58, 1791–1800.
- Villemagne, V.L., Bourgeat, P., Brown, B., Ellis, K.A., Salvado, O., Szeke, C., Macaulay, S.L., Martins, R., Maruff, P., Ames, D., Rowe, C.C., Masters, C.L., 2013. Amyloid  $\beta$  deposition, neurodegeneration, and cognitive decline in sporadic Alzheimer's disease: a prospective cohort study. *Lancet Neurol.* 12, 357–367.
- Walker, L.C., Jucker, M., 2015. Neurodegenerative diseases: expanding the prion concept. *Ann. Rev. Neurosci.* 38, 87–103.
- Walker, L.C., LeVine, H., 2012. Corruption and spread of pathogenic proteins in neurodegenerative disease. *J. Biol. Chem.* 287, 33109–33115.
- Weickenmeier, J., Kuhl, E., Gorilev, A., 2018. The multiphysics of prion-like diseases: progression and atrophy. *Phys. Rev. Lett.* 121, 158101.
- World Alzheimer Report, 2016. Improving healthcare for people living with dementia. Coverage, quality and costs now and in the future. Alzheimer's Disease International, London, 2016.